Models for Intrinsic Non-RRKM Dynamics. Decomposition of the S_N2 Intermediate Cl^-–CH_3Br

By Manikandan Paranjothy, Rui Sun, Amit Kumar Paul, and William L. Hase*

Department of Chemistry and Biochemistry, Texas Tech University, Lubbock, Texas 79409, USA

S_N2 / Non-RRKM Dynamics / Unimolecular Decomposition / Direct Dynamics

Chemical dynamics simulations, based on both an analytic potential energy surface (PES) and direct dynamics, were used to investigate the intrinsic non-RRKM dynamics of the Cl^-–CH_3Br ion-dipole complex, an important intermediate in the $Cl^- + CH_3Br$ S_N2 nucleophilic substitution reaction. This intermediate may dissociate to $Cl^- + CH_3Br$ or isomerize to the $ClCH_3$–Br^- ion-dipole complex. The decomposition of microcanonical ensembles of the Cl^-–CH_3Br intermediate were simulated, and the ensuing populations *vs.* time of the excited intermediate and $Cl^- + CH_3Br$ and $ClCH_3$–Br^- products were fit with multi-exponential functions. The intrinsic non-RRKM dynamics is more pronounced for the simulations with the analytic PES than by direct dynamics, with the populations for the former and latter primarily represented by tri- and bi-exponential functions, respectively. For the analytic PES and direct dynamics simulations, the intrinsic non-RRKM dynamics is more important for the isomerization pathway to form $ClCH_3$–Br^- than for dissociation to $Cl^- + CH_3Br$. Since the decomposition probability of Cl^-–CH_3Br is non-exponential, the Cl^-–CH_3Br unimolecular rate constant depends on pressure, with both high and low pressure limits. The high pressure limit is the RRKM rate constant and for the simulations with the analytic PES the rate constant decreased by a factor of 3.0, 5.6, and 4.3 in going from the high to low pressure limit for total energies of 40, 60, and 80 kcal/mol. For the direct dynamics simulations these respective factors are 2.4, 1.4, and 1.2. A separable phase space model with intermolecular and intramolecular complexes describes some of the simulation results, but overall models advanced for intrinsic non-RRKM dynamics give incomplete representations of the intermediate and product populations *vs.* time determined from the simulations.

1. Introduction

Rice–Ramsperger–Kassel–Marcus (RRKM) theory [1–3], derived from classical mechanics [3–5], is a limiting model for the dynamics of unimolecular decomposition. It assumes that the classical dynamics is ergodic on the time-scale of the unimolecular reaction so that a microcanonical ensemble of states is maintained for the molecules as they decompose [5]. With this assumption the unimolecular rate constant is the same for

---

* Corresponding author. E-mail: bill.hase@ttu.edu

all times of the unimolecular reaction and given by microcanonical rate theory; *i.e.*

$$k(E, J) = \frac{N^{\ddagger}(E, J)}{h\rho(E, J)} \tag{1}$$

where E is the total energy, J the total angular momentum, $N^{\ddagger}(E,J)$ the sum of states for the transition state (TS) separating the unimolecular reactant from products, and $\rho(E,J)$ the density of states for the unimolecular reactant.

　　With the assumption of a microcanonical ensemble for all times the population of the unimolecular reactant decays exponentially with a rate constant given by RRKM theory; *i.e.* [6]

$$N(t) = N(0)e^{-k(E)t} \tag{2}$$

[The rate constant also depends on angular momentum as given by Eq. (1), but to simplify the notation it is written as $k(E)$]. As described by the pioneering work of Bunker in the early 1960's [7,8], a quantity fundamental to unimolecular rate theory is the lifetime distribution $P(t)$, which according to RRKM theory is

$$P(t) = -\frac{1}{N(0)}\frac{dN(t)}{dt} = k(E)e^{-k(E)t} \tag{3}$$

The rate constant at $t = 0$ is the RRKM $k(E,J)$ for the initial microcanonical ensemble and the ensuing decomposition kinetics is also given by $k(E,J)$, since a microcanonical ensemble is assumed for all times.

　　The assumption of RRKM is that a microcanonical ensemble of states exists at $t = 0$. As discussed previously [9], it is doubtful that this assumption is actually obeyed for any experiment, including collisional activation. The essence of the RRKM assumption is that an experiment's nonrandom initial distribution of states is rapidly transformed into a microcanonical ensemble of states by the molecules' intramolecular motion. This is assumed to occur on a time scale much shorter than that for the unimolecular reaction.

　　Intrinsic non-RRKM behavior occurs when the unimolecular dynamics is not ergodic and, as a result, the initial microcanonical ensemble is not maintained during the unimolecular decomposition [9,10]. The unimolecular rate constant is then time-dependent, *i.e.*

$$k(E, t) = \frac{1}{N(t)}\frac{dN(t)}{dt} \tag{4}$$

$N(t)$ is no longer a single exponential as assumed by RRKM theory, but may be represented by a multi-exponential function as [11]

$$\frac{N(t)}{N(0)} = \sum_i f_i e^{-k_i t} \tag{5}$$

where the sum of the f_i equals unity. A likely scenario for intrinsic non-RRKM dynamics is to have three or more exponential terms in Eq. (5). The lifetime distribution for the

non-exponential $N(t)$ is

$$P(t) = \sum_i f_i k_i e^{-k_i t} \tag{6}$$

with $P(0) = \sum_i f_i k_i$ equal to the RRKM rate constant $k(E)$, since a microcanonical ensemble exists at $t = 0$. In the work presented here the intrinsic non-RRKM $N(t)$ is represented by the above multi-exponential function, but it should be noted that both power law [12–17] and stretched exponential [18] expressions have also been used to describe non-exponential unimolecular decomposition.

RRKM theory requires chaotic intramolecular dynamics, with ergodic behavior on the time-scale of the unimolecular reaction, and there is considerable interest in characterizing the type(s) of classical motions and resulting phase space structure(s) which give rise to intrinsic non-RRKM behavior [19–28]. Part of the phase space may consist of quasiperiodic trajectories, undergoing regular motion, which are trapped and cannot decompose [29,30]. Adjacent to these quasiperiodic trajectories are trajectories identified as vague tori [23,24] which undergo regular motion for long times, but ultimately decompose with lifetimes much longer than the RRKM value. The phase space for the non-ergodic dynamics of a multi-dimensional polyatomic molecule consists of an Arnold web of corridors of irregular/chaotic motion traversing interconnected regions of regular motion [26,28]. A molecular understanding of intrinsic non-RRKM dynamics desires the identification of the specific mode excitations which lead to irregular or regular atomic-level dynamics [31–35].

Both experiments and simulations have shown that the chemical dynamics of gas-phase $X^- + CH_3Y \rightarrow XCH_3 + Y^-$ S_N2 nucleophilic substitution reactions are non-statistical [36–38]. Reactions, such as $Cl^- + CH_3Br \rightarrow ClCH_3 + Br^-$, have X^-–CH_3Y and XCH_3–Y^- ion-dipole complexes separated by a central barrier and the unimolecular dynamics of these complexes are intrinsically non-RRKM. These dynamics arise from the weak coupling between the three low-frequency intermolecular modes of the complex and the complex's much higher frequency nine intramolecular modes. In the work represented here chemical dynamics simulations are performed to study details of the intrinsic non-RRKM dynamics for the Cl^-–CH_3Br complex [39–42], and the results are analyzed in terms of proposed models. RRKM rate constants for Cl^-–CH_3Br dissociation to $Cl^- + CH_3Br$ and isomerization to $ClCH_3$–Br^- are found from $t = 0$ intercepts of $P(t)$ lifetime distributions as described above. These rate constants include the full anharmonicity of the PES. The same rate constants would be obtained from Eq. (1) if accurate anharmonic effects were included for both the sum and density of states [5]. Variational RRKM theory [5] would be needed to locate the TS for Cl^-–$CH_3Br \rightarrow Cl^- + CH_3Br$ dissociation.

The remainder of this article is organized as follows. Models for intrinsic non-RRKM dynamics are described in Sect. 2. Both an analytic potential PES and direct dynamics were used for the simulations, and they are described in Sect. 3. Section 4 reports analyses of the intrinsically non-RRKM lifetime distributions obtained from the simulations. The variation of Cl^-–CH_3Br decomposition rate constants with pressure is discussed in Sect. 5. The simulation results and models for intrinsic non-RRKM dynamics are compared in Sect. 6. A summary in Sect. 7 concludes the article.
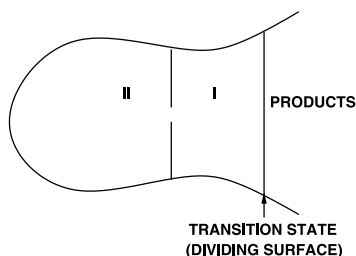
Fig. 1. Depiction of the coupled phase space model with two phase space regions (adapted from Ref. [34]).

2. Models for intrinsic non-RRKM dynamics

2.1 Coupled phase space model

In previous work Marcus *et al.* [43] presented a model in which the intramolecular phase space of the reacting molecule is represented as containing different weakly coupled regions, each with its own kinetic behavior. The weak coupling restricts intramolecular vibrational energy redistribution (IVR) [44,45], resulting in non-exponential unimolecular decomposition. Models with both two and three phase space regions were presented, with the latter more realistic for the problem considered in Ref. [36] and able to describe the trajectory results. However, the model with two phase space regions, depicted in Fig. 1, is instructive and illustrates important features of non-RRKM dynamics. The two models are identified as two-state and three-state models.

The two phase space regions for the two-state model are N_1 and N_2, and their kinetics are written as

$$N_1 \xrightarrow{k_1} \text{products} \tag{7a}$$

$$N_1 \underset{k_3}{\overset{k_2}{\rightleftharpoons}} N_2 \tag{7b}$$

where unimolecular decomposition only occurs from region N_1 and k_2 and k_3 are IVR rate constants, coupling regions N_1 and N_2. For a microcanonical ensemble at $t = 0$, $k_2 N_1(0) = k_3 N_2(0)$ and the microcanonical rate constant $k(E)$ is given by

$$k(E) = \frac{k_1 k_3}{(k_2 + k_3)} \tag{8}$$

For the initial microcanonical ensemble, the population *vs.* time, *i.e.* $N(t) = N_1(t) + N_2(t)$, is

$$\frac{N(t)}{N(0)} = \frac{e^{-\lambda_1 t}(k_1 - \lambda_2)(k_1 + k_2 + k_3 - \lambda_1) - e^{-\lambda_2 t}(k_1 - \lambda_1)(k_1 + k_2 + k_3 - \lambda_2)}{(k_2 + k_3)(\lambda_1 - \lambda_2)} \tag{9}$$

Here λ_1 and λ_2 are the eigenvalues of the linear system in Eqs. (7a) and (7b) and satisfy $\lambda_1 + \lambda_2 = k_1 + k_2 + k_3$ and $\lambda_1 \lambda_2 = k_1 k_3$. An important modification to the two-state model for the work presented here is to allow reaction from region II, *i.e.*

$$N_2 \xrightarrow{k_4} \text{products} \tag{10}$$

The microcanonical rate constant is then given by

$$k(E) = \frac{(k_1 k_3 + k_4 k_2)}{(k_2 + k_3)} \tag{11}$$

The relative population *vs.* time, $N(t)/N(0)$, for this model is most straightforwardly obtained by numerically integrating the coupled kinetic equations for Eqs. (7) and (10). This modified two-state model is referred to as the two-state-mod model.

For the three-state model the scheme in Eqs. (7a) and (7b) is supplemented with the step

$$N_1 \underset{k_5}{\overset{k_4}{\rightleftarrows}} N_3 \tag{12}$$

The microcanonical rate constant becomes

$$k(E) = \frac{k_1}{\{1 + k_2/k_3 + k_4/k_5\}} \tag{13}$$

and for this more complex system the population *vs.* time, *i.e.* $N(t) = N_1(t) + N_2(t) + N_3(t)$, is most conveniently determined by numerically integrating the coupled kinetic equations.

2.2 Separable phase space model

For the separable phase space model, each phase space region has its individual unimolecular rate constant and there is no coupling between the different regions. The population *vs.* time for the different N_i regions is then

$$N(t) = \sum_i N_i(t) = \sum_i N_i(0) f_i e^{-k_i t} \tag{14}$$

The relative population $N(t)/N(0)$ and the lifetime distribution are given by Eqs. (5) and (6), respectively. The microcanonical rate constant is $k(E) = \sum_i f_i k_i$, where f_i equals $N_i(0)/N(0)$ and the summation of the $N_i(0)$ equals $N(0)$. This model is equivalent to that for the unimolecular decomposition of a microcanonical ensemble of isolated resonance states, each decomposing exponentially [46–48].

An illustration of this model is the highly idealized situation of two phase space regions, with the trajectories trapped in one of the regions so they cannot decompose [49]. From Eq. (14), the resulting relative population *vs.* time is

$$\frac{N(t)}{N(0)} = f_1 e^{-k_1 t} + f_2 \tag{15}$$

where the rate constant k_2, for region 2, is zero. The microcanonical rate constant is then $k(E) = f_1 k_1$. For this model k_1 is a microcanonical-like rate constant, *i.e.* $k_1 = N^{\ddagger}/\rho_1$, with the decomposition transition state sum of states $N^{\ddagger}$ and a restricted density of states equal to f_1 times the total density ρ.

The k_i in Eq. (14) are microcanonical-like rate constants, *i.e.* $k_i = N_i^‡/\rho_i$, where $N_i^‡$ is the number of TS states accessible to phase space region i and the sum of the $N_i^‡$ equals the total TS sum of states $N^‡$. The fraction f_i in Eq. (14) is given by ρ_i/ρ, where the latter is the total density of states. With these definitions the sum $\sum_i f_i k_i$ is the RRKM rate constant $k(E)$.

2.3 Weakly coupled reaction coordinate model

Based on the stable states picture of chemical reactions, and a model with weak coupling between the reaction coordinate and the remaining degrees of freedom [50], a correction to the RRKM rate constant has been proposed; *i.e.*

$$k_{\mathrm{obs}}(E) = \kappa k(E) \tag{16}$$

where, as discussed above, $k(E)$ is the RRKM rate constant. The correction factor κ is given by [51,52]

$$\kappa = \frac{k_{\mathrm{IVR}}}{k_{\mathrm{IVR}} + \nu_R} \tag{17}$$

where k_{IVR} is an IVR rate constant and ν_R is the reaction coordinate vibrational frequency (*i.e.* the barrier-crossing frequency). The κ factor equals unity if $k_{\mathrm{IVR}} \gg \nu_R$. The relationship of this model to intrinsic non-RRKM dynamics and the non-RRKM lifetime distribution, Eq. (6), is uncertain. For intrinsic non-RRKM dynamics, $P(t)$ is non-exponential and the unimolecular rate constant depends on time. If the non-RRKM $P(t)$ is bi-exponential with $f_1 \gg f_2$ and $k_1 \gg k_2$, then, after the initial short-time decomposition one would have $P(t) \sim k_2 e^{-k_2 t}$. It is possible that $k_{\mathrm{obs}}(E)$ in Eq. (16) is equivalent to k_2.

If $P(t)$ is bi-exponential and k_2 equals the above $k_{\mathrm{obs}}(E)$, the values for k_1 and the f's are not obvious. One possible value for k_1 is ν_R, but that leads to the questionable expression $[(k_{\mathrm{IVR}} + \nu_R)/(k_{\mathrm{IVR}} - \nu_R^2/(k(E) - \nu_R))]$ for f_2 with f_1 plus f_2 equal to unity. It certainly would be of interest to establish the relationship of $k_{\mathrm{obs}}(E)$ to the parameters for a bi-exponential $P(t)$.

3. Methodologies for the analytic PES and direct dynamics simulations

Unimolecular decomposition of $Cl^- - CH_3Br$ is studied using both an analytic PES and by direct dynamics simulations. The sections below describe the analytic PES and the direct dynamics simulation methodologies.

3.1 Analytic potential energy surface

The multi-dimensional analytic PES, *i.e.* PES1(Br), for the $Cl^- + CH_3Br$ S$_N$2 reaction was developed by Wang *et al.* [39,53] and has been described in considerable detail in previous publications. The energies and harmonic vibrational frequencies of the stationary points on the PES are provided in the supporting information. Figure 2 shows the
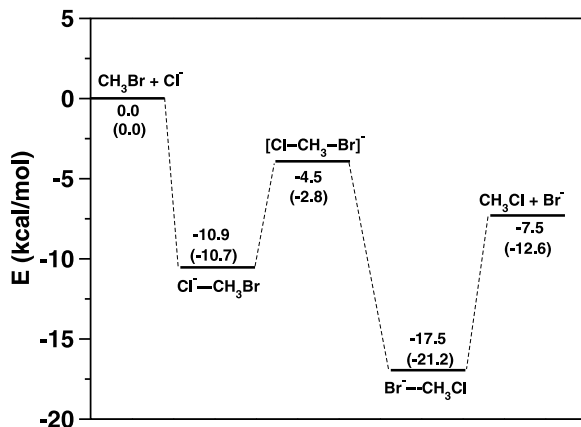
Fig. 2. Schematic representation of the potential energy surface of the S_N2 reaction $CH_3Br + Cl^- \rightarrow CH_3Cl + Br^-$, calculated at PBE0/6-31++g**/ECP(Br) level of theory. The values in parentheses describe the analytic PES values (Ref. [44]).

reaction path potential and stationary point energies on the PES. This analytic potential energy function and its derivatives are incorporated into the general chemical dynamics computer program VENUS [54,55] which is used in the trajectory simulations reported here.

The pre-reaction ion-dipole complex Cl^-–CH_3Br is sampled with classical micro-canonical sampling [56,57] at fixed total energies of $E = 40$, 60 and 80 kcal/mol. The rotational temperature was kept at 300 K with $E_{rot} = 3RT/2$. Ensembles of 5000 trajectories were time propagated at each energy until all of the complexes either iso-merized to the $ClCH_3$–Br^- complex or dissociated to $Cl^- + CH_3Br$. The trajectories were analyzed for the lifetime of the Cl^-–CH_3Br complex. If the trajectories disso-ciated to the $Cl^- + CH_3Br$ reactants, the lifetime was taken as the time of the last inner turning point in the $Cl^- + CH_3Br$ relative motion before dissociation. For isomer-ization to the $ClCH_3$–Br^- ion-dipole complex, the lifetime was taken as the time the trajectory crossed the $[Cl$–CH_3–$Br]^-$ central barrier. After isomerization, recrossings of the trajectories back to the Cl^-–CH_3Br complex were not considered in the present work.

3.2 Direct dynamics

To identify an appropriate electronic structure theory to be used in direct dynamics simulations [58–60], the stationary points on the $Cl^- + CH_3Br$ S_N2 reaction potential energy surface were characterized with various levels of electronic structure theory. Energies and harmonic vibrational frequencies of the stationary points found by dif-ferent levels of electronic structure theory are presented in the supporting information. By considering both speed and accuracy, we chose the PBE0/6-31++g**/ECP(Br) level of theory for the direct dynamics simulations. Figure 2 shows the stationary point energies computed at this level of theory. The energy of the ion-dipole complex Cl^-–CH_3Br is -10.9 kcal/mol with respect to the separated reactants ($Cl^- + CH_3Br$). For

the analytical PES this energy is -10.7 kcal/mol. The central barrier separating the pre-reaction and post-reaction ion-dipole complexes lies below the separated reactants by 4.5 kcal/mol and the barrier height is 6.4 kcal/mol from the Cl$^-$–CH$_3$Br ion-dipole complex. These energies are 2.8 and 7.9 kcal/mol, respectively, for the analytic PES. Since the Cl$^-$–CH$_3$Br $\rightarrow$ ClCH$_3$–Br- isomerization barrier is lower for the DFT PES, than for the analytic PES, more isomerization is expected for the DFT direct dynamics simulations.

Similar to the analytic PES calculations, the ion-dipole complex Cl$^-$–CH$_3$Br was excited with classical microcanonical sampling at total energies of $E = 40$, 60 and 80 kcal/mol. The rotational temperature was kept at 300 K, with $E_{rot} = 3RT/2$. At each energy, 500 trajectories were propagated to a total integration time of 15 ps. The direct dynamics simulations were performed using the chemical dynamics program VENUS interfaced with the electronic structure theory package NWChem [61,62]. Default criteria [61,62] were used for the electronic structure calculations required for the direct dynamics simulations. Average energies and mean average energy variations for the simulations are presented in the supporting information. For $E = 60$ and 80 kcal/mol, all of the trajectories either isomerized or dissociated to reactants. However, at $E = 40$ kcal/mol, only 82% of the trajectories either isomerized or dissociated and rest of the trajectories remained in the Cl$^-$–CH$_3$Br complex well when the trajectories were halted at 15 ps. Similar to the analytic PES simulations, for those trajectories which isomerize, the time at which a trajectory crosses the central barrier is taken as the lifetime. For those trajectories which dissociate to Cl$^-$ + CH$_3$Br reactants, the time at which the C–Cl distance reaches 12 Å is defined as the lifetime of the trajectory.

4. Simulation results

The vibrationally excited Cl$^-$–CH$_3$Br intermediate may either isomerize to the ClCH$_3$–Br$^-$ intermediate, identified Pr_1, or dissociate to Cl$^-$ + CH$_3$Br, Pr_2. The results presented and analyzed below are the relative number of Cl$^-$–CH$_3$Br intermediates remaining *vs.* time, $N(t)/N(0)$, and the relative number of products formed *vs.* time, $Pr_1(t)/N(0)$ and $Pr_2(t)/N(0)$. Previous simulations [38,39] have shown that the Cl$^-$–CH$_3$Br $\rightarrow$ ClCH$_3$–Br$^-$ isomerization dynamics includes extensive recrossings of the [Cl–CH$_3$–Br]$^-$ central barrier, *i.e.* transition state (TS), separating Cl$^-$–CH$_3$Br and ClCH$_3$–Br$^-$. These dynamics are not investigated here and isomerization is assumed to have occurred when the reactive system reaches this central barrier.

To analyze the simulations, the relative number of Cl$^-$–CH$_3$Br intermediates *vs.* time was fit with Eq. (5). If all the intermediates decompose in the simulation, the initial number of intermediates equals the final number of products; *i.e.* $N(0) = Pr_1(\infty) + Pr_2(\infty)$. These dynamics were obtained except for the direct dynamics at 40 kcal/mol. The relative numbers of intermediates and products are related by $N(t)/N(0) = 1 - Pr_1(t)/N(0) - Pr_2(t)/N(0)$. As is done for the intermediates, the relative number of products *vs.* time is fit by a multi-exponential function; *e.g.*

$$\frac{Pr_1(t)}{N(0)} = c_1 \left[1 - \sum f_{1i} e^{-k_{1i}t} \right] \tag{18}$$
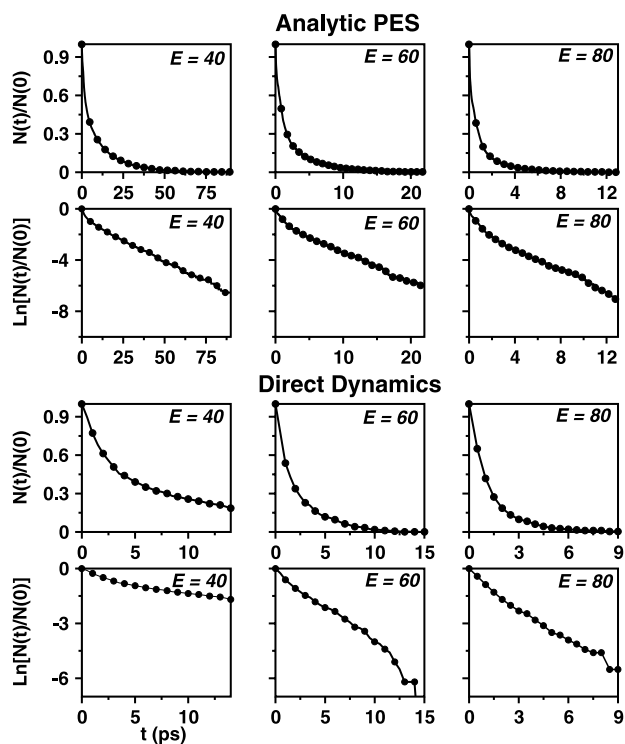
Fig. 3. Lifetime distribution, $N(t)/N(0)$ and $\ln[N(t)/N(0)]$ *vs.* time t (in ps), determined by the analytic PES and direct dynamics simulations. The energy, E, is in units of kcal/mol.

where $c_1 = Pr_1(\infty)/N(0)$, $c_2 = Pr_2(\infty)/N(0)$, and $c_1 + c_2 = 1$. In terms of product formation, $N(t)/N(0)$ is given by

$$\frac{N(t)}{N(0)} = c_1 \sum f_{1i} e^{-k_{1i}t} + c_2 \sum f_{2i} e^{-k_{2i}t} \tag{19}$$

where the sum of the f_{1i} and also the f_{2i} equal unity. Comparisons show that the fits to $N(t)/N(0)$ with Eqs. (5) and (19) are identical within statistical uncertainties.

In the following the simulation results, and their analyses, obtained with the analytic PES and by direct dynamics are presented.

4.1 Analytic PES dynamics

Plots of $N(t)/N(0)$ and $\ln[N(t)/N(0)]$ are given in Fig. 3 for the simulations with the analytic PES. Fits to the trajectory $N(t)/N(0)$ require a tri-exponential function and the fitting parameters are listed in Table 1. For the 40 kcal/mol simulations, the fractions of the three components to the tri-exponential function are similar in size, while the middle component is a factor of two larger than the others for E of 60 and 80 kcal/mol.

Table 1. Parameters for fits to the simulation $N(t)/N(0)$ distributions[a].

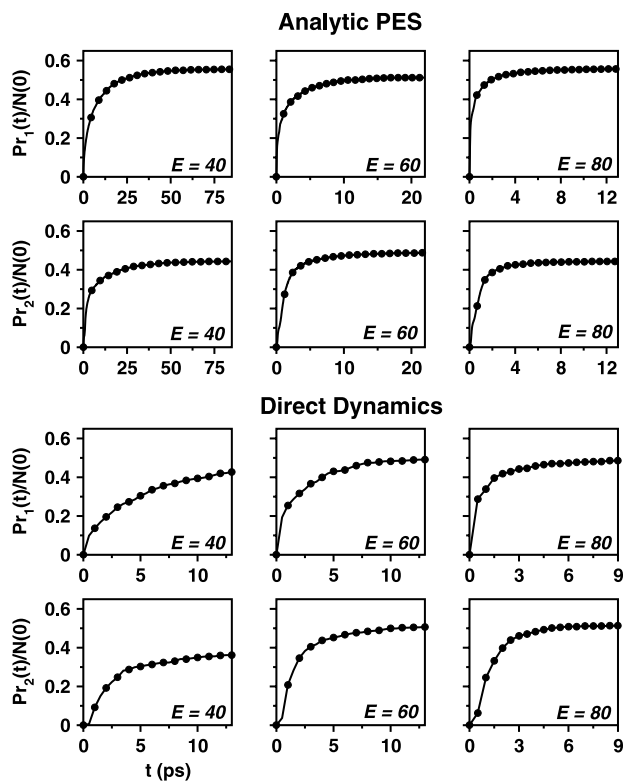| | Energy | | |
	40	60	80
		Analytic PES	
f_1	0.389	0.108	0.229
f_2	0.238	0.599	0.616
f_3	0.373	0.293	0.155
k_1	0.817	20.51	17.46
k_2	0.174	1.042	1.440
k_3	0.062	0.216	0.356
		Direct dynamics	
f_1	0.511	0.457	0.796
f_2	0.489	0.543	0.204
f_3	–	–	–
k_1	0.506	1.047	1.044
k_2	0.067	0.313	0.391
k_3	–	–	–

[a] The fits are to Eq. (5). The sum of f_1, f_2 and f_3 is set to unity in the fitting, and the k's are in units of ps^{-1}. The energies are in kcal/mol.

The values for the three fitted k_i vary by factors of ~10, 100, and 50 for E of 40, 60 and 80 kcal/mol, respectively.

The relative numbers of Pr_1 products, $ClCH_3$–Br^-, and Pr_2 products, $Cl^- + CH_3Br$, *vs.* time are plotted in Fig. 4. For each energy, $Pr_1(t)/N(0)$ is fit by a tri-exponential function, while $Pr_2(t)/N(0)$ is fit by a bi-exponential function for E of 60 and 80 kcal/mol. The non-RRKM dynamics for the Cl^-–$CH_3Br \rightarrow ClCH_3$–$Br^-$ pathway is more non-RRKM with the k_i values varying by a factor of ~50 for each of the energies. Each component in the tri-exponential is an important contributor. For formation of the $Cl^- + CH_3Br$ products there is only one dominant component in $Pr_2(t)/N(0)$ for E of 60 and 80 kcal/mol, while there are two nearly equal components of ~0.5 for E of 40 kcal/mol. For this pathway the k_i for the two dominant components vary by factor of ~10 at 40 kcal/mol, and for 60 and 80 kcal/mol the two k_i vary by approximately a factor of 5.

4.2 Direct dynamics

For the direct dynamics simulations the plots of $N(t)/N(0)$ and $\ln[N(t)/N(0)]$ are given in Fig. 3. A bi-exponential function is required to fit the trajectory $N(t)/N(0)$ and the fitting parameters are listed in Table 1. For the 40 and 60 kcal/mol simulations, the fractions for the two components are similar in size, while for the 80 kcal/mol simulations the fraction for the bigger rate constant is substantially larger. The ratio between the rate constants for the two components decreases in going from E of 40 to 60 and 80 kcal/mol; *i.e.* it is ~8, 3, and 3 for $E = 40$, 60, and 80 kcal/mol, respectively.

Fig. 4. The relative number of products, Pr_1 ($ClCH_3–Br^-$) and Pr_2 ($Cl^- + CH_3Br$) *vs.* time t (in ps), determined by the analytic PES and direct dynamics simulations. The energy, E, is in units of kcal/mol.

The relative numbers of Pr_1 products, $ClCH_3–Br^-$, and Pr_2 products, $Cl^- + CH_3Br$, *vs.* time are plotted in Fig. 4. For the 40 kcal/mol simulations not all of the $Cl^-–CH_3Br$ complexes decomposed and the analyses of $Pr_1(t)$ and $Pr_2(t)$ with Eq. (18) could not be made. For E of 60 kcal/mol a bi-exponential function fits both $Pr_1(t)$ and $Pr_2(t)$, while for 80 kcal/mol $Pr_1(t)$ remains a bi-exponential but $Pr_2(t)$ becomes a single exponential. For $Pr_1(t)$ both components of the bi-exponential have significant weights, while the component with the largest rate constant dominates the bi-exponential for $Pr_2(t)$. The non-exponential character is more pronounced for $Pr_1(t)$ with the rate constants varying by factors of 16 ($E = 60$ kcal/mol) and 8 ($E = 80$ kcal/mol), while the rate constants only vary by a factor of 3 ($E = 60$ kcal/mol) for the $Pr_2(t)$ bi-exponential.

4.3 Comparison of analytic PES and direct dynamics simulations

The intrinsic non-RRKM dynamics is more pronounced for the simulations with the analytic PES than by direct dynamics. The $N(t)/N(0)$ populations for the analytic PES are fit by a tri-exponential with k_i values which vary by up to a factor of 100. For the direct

dynamics, $N(t)/N(0)$ is fit by a bi-exponential with the largest variation in the k_i a factor of 8.

For both the analytic PES and direct dynamics simulations, the non-exponential dynamics is more significant for $Pr_1(t)$, $ClCH_3$–Br^- formation, than for $Pr_2(t)$, $Cl^- + CH_3Br$ formation. However, for both $Pr_1(t)$ and $Pr_2(t)$ the analytic PES's non-exponential dynamics is more pronounced than that for the direct dynamics. To illustrate, for the analytic PES $Pr_1(t)$ is a tri-exponential with the k_i's varying by a factor of 50 for each of the energies, while for the direct dynamics $Pr_1(t)$ is a bi-exponential with k_i's varying by only a factor of 16. The differences between the analytic PES and direct dynamics $Pr_2(t)$ are relatively small.

5. The Cl^-–CH_3Br decomposition rate constant *vs.* pressure

One may directly measure $N(t)$, the population of monoenergetic reactant molecules *vs.* time [63], but often one measures the collision-averaged unimolecular rate constant [64]. If $N(t)$ is exponential, the unimolecular rate constant will be independent of pressure and equal the RRKM rate constant $k(E)$ [10]. However, if $N(t)$ is non-exponential, the unimolecular rate constant varies *vs.* pressure [11,43,65]. To relate the non-exponential $N(t)$ to experiment, it is important to calculate the resulting pressure dependent unimolecular rate constant. As shown in previous work [4,11,66], the rate constant *vs.* collision frequency (*i.e.* proportional to pressure) is given by

$$k = \omega \int_0^\infty W(t) P(t)\, dt \left/ \left\{ 1 - \int_0^\infty W(t) P(t)\, dt \right\} \right. \tag{20}$$

where ω is the collision frequency and $W(t)$ is the probability the reactant avoids a collision for time t, which is

$$W(t) = \exp(-\omega t) \tag{21}$$

if the collisions are random and thus uncorrelated. The high pressure limiting rate constant k^∞ is $P(0)$ and for the low pressure limit the rate constant is given by the expression [43]
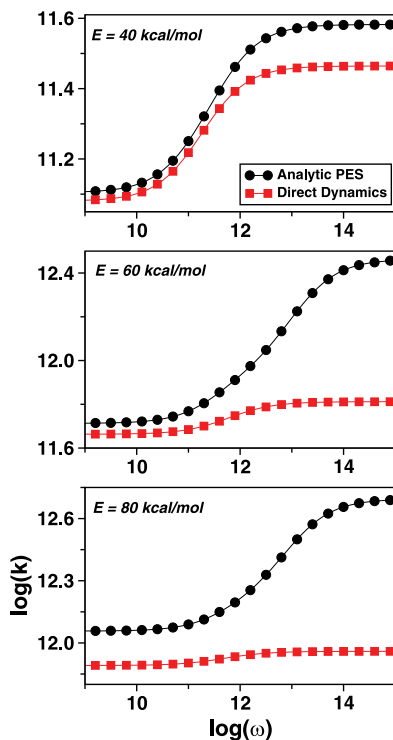
$$k^0 = N(0) \left/ \int_0^\infty N(t)\, dt \right. \tag{22}$$

For a multi-exponential $P(t)$, Eq. (6), the unimolecular rate constant *vs.* ω is given by

$$k = \omega \frac{\sum_i f_i k_i / (\omega + k_i)}{1 - \sum_i f_i k_i / (\omega + k_i)} \tag{23}$$

The expressions for k in the high and low pressure limits are

$$k^\infty = \sum_i f_i k_i \tag{24}$$

Fig. 5. Plot of logarithmic rate constant k [Eq. (23)], *vs.* logarithmic collision frequency ω, determined by the analytic PES and direct dynamics simulations.

and

$$k^0 = \frac{1}{\sum_i f_i/k_i} \qquad (25)$$

If the initial ensemble is microcanonical, the high pressure limiting rate constant is the RRKM rate constant [43].

Plots of $\log(k)$ *vs.* $\log(\omega)$ are given in Fig. 5 for both the analytic PES and direct dynamics simulations. A both interesting and important result is that the extensive variation in the k_i for the multi-exponential fits to the $N(t)/N(0)$ populations are not apparent in the collision-averaged rate constant. To illustrate, for the 60 kcal/mol simulations with the analytic PES the k_i in the tri-exponential fit to $N(t)/N(0)$ vary by ~100, but the collision averaged rate constant only varies by a factor of six. Such insensitivity of the collision-averaged rate to the multi-exponential attributes of $N(t)/N(0)$ has been discussed previously [11].

It is seen from Fig. 5 that variation in k with ω for the analytic PES is more pronounced as compared to that for the direct dynamics. For the energies of 40, 60, and 80 kcal/mol the variations in the high and low pressure limiting rate constants for the analytic PES are 3.0, 5.6, and 4.3, respectively. For the direct dynamics these respective fractions are 2.4, 1.4, and 1.2.

6. Comparison of the simulation results with models for intrinsic non-RRKM dynamics

From both chemical dynamics simulation and experimental studies, the non-RRKM dynamics of the $X^- - CH_3Y$ complex have been interpreted in terms of weak coupling between the complex's three intermolecular modes and the nine higher frequency intramolecular modes [36–38]. The complex has been referred to as either an inter-molecular or intramolecular complex, depending on which modes are excited. The intermolecular and intramolecular complexes preferentially dissociate to $X^- + CH_3Y$ and isomerize to $XCH_3 - Y^-$, respectively. This model for the $X^- - CH_3Y$ non-RRKM dynamics is consistent with the lifetime and/or lifetime distribution of $X^- - CH_3Y$ dissociation following $X^- + CH_3Y$ association [63,65,67–69], the dissociation dynamics following excitation of the intermolecular and intramolecular modes of $X^- - CH_3Y$ [39, 70], and the recrossing dynamics of the $[X - CH_3 - Y]^-$ central barrier [39,71,72].

The different dynamics observed in the simulations, for forming the $Cl^- + CH_3Br$ dissociation and $ClCH_3 - Br^-$ isomerization products, are qualitatively consistent with the above model of intermolecular and intramolecular complexes. The most pronounced example of a model with these two complexes is the separable phase space model, for which one phase space region dissociates to $Cl^- + CH_3Br$ and the other isomerizes to $ClCH_3 - Br^-$. The 80 kcal/mol direct dynamics simulations are most supportive of this model. The $Cl^- + CH_3Br$ dissociation products Pr_2 are formed exponentially, indicating the dynamics of these trajectories is statistical. In contrast, the isomerization dynamics is non-exponential, indicative of weak coupling within the phase space of these trajectories. The statistical RRKM-like rate constant for formation of the Pr_2 products is $k_2(E) = N_d^{\ddagger}/\rho_2(E)$, where $N_d^{\ddagger}$ is the number of states for the dissociation transition state and $\rho_2(E)$ is the density of states for the restricted region of phase space in which the dissociating trajectories move. This rate constant is given by $k_1 = 0.669 \, ps^{-1}$ in Table 2. In contrast the dissociation RRKM rate constant, determined from the $t = 0$ limit of the lifetime distribution for $Cl^- + CH_3Br$ formation, is $0.345 \, ps^{-1}$. The RRKM rate constant is expected to be smaller since it is based on the total $Cl^- - CH_3Br$ density of states $\rho(E)$, while $k_2(E)$ is based on the smaller density of states $\rho_2(E)$ for the restricted region of phase space. The fraction of the trajectories which dissociate is 0.52 which should approximate $\rho_2(E)/\rho(E) = 0.345/0.669 = 0.52$. The bi-exponential population distribution $Pr_1(t)$, for formation of the $ClCH_3 - Br^-$ isomerization products, may be fit nearly exactly by the coupled phase space model, Eqs. (7)–(9), and the resulting fitted rate constants for the model are $k_1 = 6.102 \, ps^{-1}$, $k_2 = 0.508 \, ps^{-1}$, and $k_3 = 0.675 \, ps^{-1}$. The smaller values of k_2 and k_3, as compared to k_1, are expected since the isomerization dynamics is not exponential with rapid IVR within the restricted region of phase space. The similar values for k_2 and k_3 are consistent with the similar fractions, *i.e.* 0.536 and 0.464, for the two components of the bi-exponential $Pr_1(t)$.

For the direct dynamics simulations at 60 kcal/mol and the analytic PES simulations at 60 and 80 kcal/mol, $Pr_2(t)$ is approximately a single exponential and the $Cl^- - CH_3Br$ unimolecular dynamics may be similar to those described above. However, the model which is appropriate for these three simulations is uncertain, since the small component in the bi-exponential $Pr_2(t)$ may arise from either weak coupling between

Table 2. Parameters for fits to the simulation $Pr_1(t)/N(0)$ and $Pr_2(t)/N(0)$ distributions.

|	$Pr_1(t)/N(0)$			$Pr_2(t)/N(0)$		
Energy	40	60	80	40	60	80
			Analytic PES			
f_1	0.172	0.276	0.468	0.582	0.824	0.923
f_2	0.359	0.329	0.352	0.408	0.176	0.077
f_3	0.469	0.395	0.180	0.010	–	–
k_1	3.116	15.50	16.83	0.605	0.818	1.164
k_2	0.283	1.508	1.738	0.066	0.183	0.273
k_3	0.069	0.248	0.375	0.031	–	–
			Direct Dynamics			
f_1	–	0.314	0.536	–	0.876	1.0
f_2	–	0.686	0.464	–	0.124	–
f_3	–	–	–	–	–	–
k_1	–	5.244	4.380	–	0.578	0.669
k_2	–	0.327	0.551	–	0.195	–
k_3	–	–	–	–	–	–

the phase space regions of the intermolecular and intramolecular complexes or weak coupling within the phase space of the intermolecular complex.

For the 40 kcal/mol analytic PES simulations, the $N(t)/N(0)$, $Pr_1(t)/N(0)$, and $Pr_2(t)/N(0)$ distributions are all tri-exponentials, with $Pr_2(t)/N(0)$ an approximate bi-exponential. An attempt was made to fit these simulations with the two-state coupled phase space model, Eq. (7), with two decomposition pathways, Eq. (10), to represent Cl^-–CH_3Br dissociation to $Cl^- + CH_3Br$ and isomerization to $ClCH_3$–Br^-. The fit was obtained by a simultaneous non-linear least squares fit to $Pr_1(t)/N(0)$ and $Pr_2(t)/N(0)$. As shown in Fig. 6, this fit is only partially successful. The fitted rate constants are $k_1 = 0.178$ ps^{-1}, $k_2 = 1.40$ ps^{-1}, $k_3 = 1.80$ ps^{-1}, and $k_4 = 0.183$ ps^{-1}. The order of magnitude larger values for k_2 and k_3, as compared to k_1 and k_4, suggests that a microcanonical ensemble of states is maintained for N_1 and N_2 during the unimolecular decomposition and $N(t)$ should be exponential. As shown in Fig. 6 this is indeed the case, and the exponential $N(t)$ resulting from the fit to $Pr_1(t)/N(0)$ and $Pr_2(t)/N(0)$ does not represent the non-exponential $N(t)$ found from the simulations.

An accurate fit would require the use of a more detailed model as discussed in Sect. 2.1. One approach would be to include an additional phase space region between N_1 and N_2; i.e.

$$N_1 \underset{k_3}{\overset{k_2}{\rightleftarrows}} N_3 \underset{k_5}{\overset{k_4}{\rightleftarrows}} N_2 \qquad (26)$$
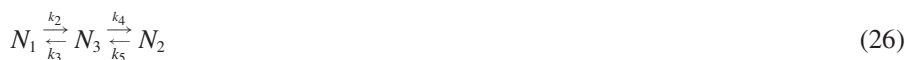
Such a model is consistent with trapping of trajectories in the central barrier of the PES [71,72]. Another approach would be to couple an additional phase space region to N_1, as in Eq. (12), since dissociation to form the $Cl^- + CH_3Br$ products is more non-exponential than isomerization to form $ClCH_3$–Br^-. The current simulations do not provide sufficient information to identify which of these two modified models is more appropriate. In addition, as discussed above, these 40 kcal/mol analytic PES simula-
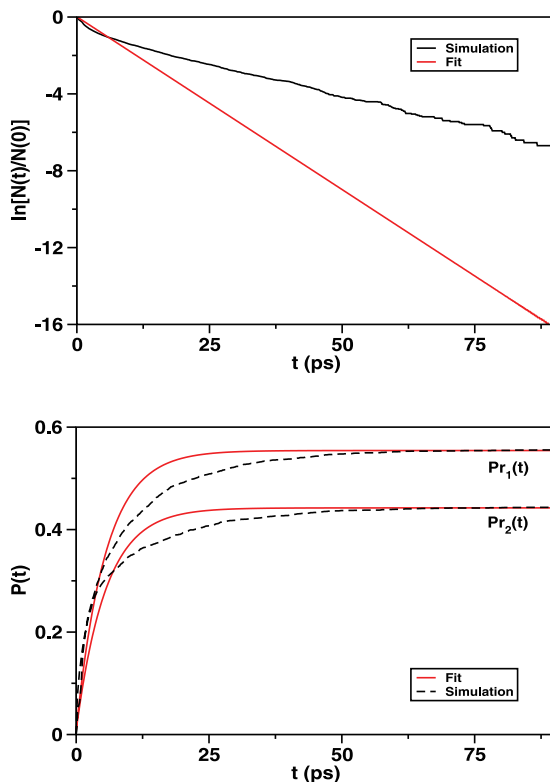
Fig. 6. Comparisons of fits, to the results of the 40 kcal/mol simulations with the analytic PES, using the coupled phase space model based on Eqs. (7) and (10).

tions could also be fit by a separable phase space model with weak coupling within the intermolecular and intramolecular complex phase space regions, with a two-state model for the intermolecular complex and a three-state model for the intramolecular complex. Without additional information regarding possible coupling between the intermolecular and intramolecular phase space regions, application of this separable phase space model does not seem warranted.

7. Summary

Previous work [34–36] has shown that the X^-–CH_3Y ion-dipole complex, important in $X^- + CH_3Y \rightarrow XCH_3 + Y^-$ S_N2 nucleophilic substitution reactions, has intrinsic non-RRKM unimolecular dynamics. Both experiments [35,36] and simulations [34,36] suggest these dynamics arise from weak coupling between the three low frequency intermolecular modes and nine high frequency intramolecular modes of the complex. Excitation of these two sets of modes forms intermolecular and intramolecular complexes, which preferentially dissociate to $X^- + CH_3Y$ and isomerize to the XCH_3–Y^-

ion-dipole complex, respectively. In the work reported here the intrinsic non-RRKM dynamics for the Cl$^-$–CH$_3$Br complex were studied by chemical dynamics simulations utilizing an analytic PES and by direct chemical dynamics.

The results of the simulations are qualitatively consistent with a model consisting of two separable or weakly coupled regions of phase space, comprising intermolecular and intramolecular complexes. The unimolecular population of the Cl$^-$–CH$_3$Br complex is multi-exponential, in contrast to the RRKM prediction of exponential decay, with rate constants for the multi-exponential which vary as much as a factor of 100. The multi-exponential, non-RRKM behavior is more for the ClCH$_3$–Br$^-$ isomerization pathway than for the Cl$^-$ + CH$_3$Br dissociation pathway. The analytic PES and direct dynamics simulations give similar dynamics for forming the Cl$^-$ + CH$_3$Br. However, the analytic PES simulations give dynamics for the ClCH$_3$–Br$^-$ pathway which are substantially more non-RRKM than found by the direct dynamics simulations.

The populations of the Cl$^-$–CH$_3$Br complex and Cl$^-$ + CH$_3$Br and ClCH$_3$–Br$^-$ products *vs.* time, obtained from the simulations, were compared with models of intrinsic non-RRKM dynamics. At the highest energy study of 80 kcal/mol for the direct dynamics simulations, a separable phase space model describes the Cl$^-$–CH$_3$Br unimolecular dynamics. The population of the Cl$^-$ + CH$_3$Br products *vs.* time is represented by exponential unimolecular decomposition, consistent with microcanonical-like dynamics for an intermolecular complex restricted region of phase space. In contrast, the unimolecular dynamics is multi-exponential for the ClCH$_3$–Br$^-$ pathway, suggesting a weakly coupled region of phase space for the intramolecular complex. Similar dynamics is observed for the Cl$^-$ + CH$_3$Br for the direct dynamics simulations at 60 kcal/mol, and the analytic PES simulations at 60 and 80 kcal/mol, however, the dynamics for this pathway are bi-exponential with an additional component with a small fraction. It is uncertain whether this additional component in the Cl$^-$ + CH$_3$Br population *vs.* time arises from coupling between the intermolecular and intramolecular complexes, or inefficient IVR for the intermolecular complex. The extensive multi-exponential, non-RRKM dynamics observed for both the dissociation and isomerization pathways at 40 kcal/mol may arise from inefficient IVR dynamics for the intermolecular and intramolecular complexes and/or weak coupling between these complexes. More work needs to be done to develop tractable and representative models of intrinsic non-RRKM dynamics.

For the Cl$^-$–CH$_3$Br unimolecular dynamics reported here, isomerization to ClCH$_3$–Br$^-$ was assumed to have occurred when the trajectory attained the [Cl–CH$_3$–Br]$^-$ central barrier connecting the Cl$^-$–CH$_3$Br and ClCH$_3$–Br$^-$ potential energy minima. The lifetime distribution for attaining the central barrier, obtained from the simulations, was compared with the prediction of RRKM theory. In future work it will be of interest to extend the current simulation to include an investigation of the ClCH$_3$–Br$^-$ unimolecular dynamics after crossing the central barrier. Previous simulations [38,39] have shown that, after the excited Cl$^-$–CH$_3$Br intermediate crosses the central barrier, there may be extensive recrossings of this barrier. It would be of interest to study these dynamics, as well as the dynamics for ClCH$_3$–Br$^-$ dissociation to the ClCH$_3$ + Br$^-$ products. The latter are expected to be intrinsically non-RRKM.

For the model simulations reported here, the Cl$^-$–CH$_3$Br intermediate has a low rotational energy of $3RT/2$, $T = 300$ K, and a resulting low total angular momentum.

Formation of this intermediate by Cl⁻–CH₃Br collisions occurs at large impact parameters and a resulting large total angular momentum [64]. In future simulations, it would be of interest to investigate how such large angular momenta affect the Cl⁻–CH₃Br unimolecular dynamics. This may be done by extending the current simulations to microcanonical ensembles with large angular momenta.

Acknowledgement

References

1. R. A. Marcus and O. K. Rice, J. Phys. Colloid Chem. **55** (1951) 894.
2. R. A. Marcus, J. Chem. Phys. **20** (1952) 359.
3. H. M. Rosenstock, M. B. Wallenstein, A. L. Wahrhaftig, and H. Eyring, P. Natl. Acad. Sci. USA, **38** (1952) 667.
4. W. Forst, *Theory of Unimolecular Reactions*, Academic Press, New York (1973).
5. T. Baer and W. L. Hase, *Unimolecular Reaction Dynamics. Theory and Experiments*, Oxford, New York (1996).
6. W. L. Hase, Dynamics of Molecular Collisions, Part B, in: *Modern Theoretical Chemistry*, Vol. 2, W. H. Miller (Ed.), Plenum, New York (1976), pp. 121–170.
7. D. L. Bunker, J. Chem. Phys. **37** (1962) 393.
8. D. L. Bunker, J. Chem. Phys. **40** (1964) 1946.
9. D. L. Bunker and W. L. Hase, J. Chem. Phys. **59** (1973) 4621.
10. U. Lourderaj and W. L. Hase, J. Phys. Chem. A **113** (2009) 2236.
11. W. L. Hase, R. J. Duchovic, K. N. Swamy, and R. J. Wolf, J. Chem. Phys. **80** (1984) 714.
12. S. A. Schofield and P. G. Wolynes, J. Chem. Phys **98** (1993) 1123.
13. S. A. Schofield, R. E. Wyatt and P. G. Wolynes, J. Chem. Phys **105** (1996) 940.
14. S. Keshavamurthy, Chem. Phys. Lett. **300** (1999) 281.
15. V. Wong and M. Gruebele, J. Phys. Chem. A **103** (1999) 10083.
16. A. Semparithi and S. Keshavamurthy, J. Chem. Phys **125** (2006) 141101.
17. S. Keshavamurthy, Int. Rev. Phys. Chem. **26** (2007) 521.
18. G. S. Ezra, H. Waalkens and S. Wiggins, J. Chem. Phys **130** (2009) 164118.
19. D. W. Oxtoby and S. A. Rice, J. Chem. Phys. **65** (1976) 1676.
20. C. Jaffé and P. Brumer, J. Chem. Phys. **73** (1980) 5646.
21. G. Hose and H. S. Taylor, J. Chem. Phys. **76** (1982) 5356.
22. E. L. Sibert III, W. P. Reinhardt, and J. T. Hynes, J. Chem. Phys. **77** (1982) 3583.
23. C. Jaffé and W. P. Reinhardt, J. Chem. Phys. **77** (1982) 5191.
24. R. B. Shirts and W. P. Reinhardt, J. Chem. Phys. **77** (1982) 5204.
25. J. Brickmann, R. Pfeiffer, and P. C. Schimidt, Ber. Bunsenges. Phys. Chem. **88** (1984) 382.
26. G. S. Ezra, Classical Trajectory Studies of Intramolecular Dynamics: Local Mode Dynamics, Rotation–Vibration Interaction and the Structure of Multidimensional Phase Space, in: *Advances in Classical Trajectory Methods*, Vol. 1, W. L. Hase (Ed.), JAI, London (1992), pp. 1–40.

27. M. J. Davis, Int. Rev. Phys. Chem. **14** (1995) 15.
28. S. Keshavamurthy and G. S. Ezra, J. Chem. Phys. **107** (1997) 156.
29. W. L. Hase, J. Phys. Chem. **86** (1982) 2873.
30. R. J. Duchovic, K. N. Swamy, and W. L. Hase, J. Chem. Phys. **80** (1984) 1462.
31. G. S. Ezra, H. Waalkens, and S. Wiggins, J. Chem. Phys. **130** (2009) 164118.
32. G. S. Ezra and S. Wiggins, J. Phys. A-Math. Theor. **42** (2009) 205101.
33. P. Collins, G. S. Ezra, and S. Wiggins, J. Chem. Phys. **133** (2010) 014105.
34. P. Manikandan and S. Keshavamurthy, J. Chem. Phys. **127** (2007) 064303.
35. P. Manikandan, A. Semparithi, and S. Keshavamurthy, J. Phys. Chem. A **113** (2009) 1717.
36. W. L. Hase, Science **266** (1994) 998.
37. M. L. Chabinyc, S. L. Craig, C. K. Regan, and J. I. Brauman, Science **279** (1998) 1882.
38. P. Manikandan, J. Zhang, and W. L. Hase, J. Phys. Chem. A **116** (2012) 3061.
39. H. Wang, G. H. Peslherbe, and W. L. Hase, J. Am. Chem. Soc. **116** (1994) 9644.
40. G. H. Peslherbe, H. Wang, and W. L. Hase, J. Am. Chem. Soc. **118** (1996) 2257.
41. H. Wang and W. L. Hase, Chem. Phys. **212** (1996) 247.
42. P. Manikandan and W. L. Hase, J. Chem. Phys. **136** (2012) 184110.
43. R. A. Marcus, W. L. Hase, and K. N. Swamy, J. Phys. Chem. **88** (1984) 6717.
44. W. L. Hase, J. Phys. Chem. **90** (1986) 365.
45. T. Uzer and W. H. Miller, Phys. Rep. **199** (1991) 73.
46. W. H. Miller, Chem. Rev. **87** (1987) 19.
47. W. L. Hase, S.-W. Cho, D.-H Lu, and K. N. Swamy, Chem. Phys. **139** (1989) 1.
48. D. H. Lu and W. L. Hase, J. Phys. Chem. **93** (1989) 1681.
49. W. L. Hase, D. G. Buckowski, and K. N. Swamy, J. Phys. Chem. **87** (1983) 2754.
50. S. H. Northrup and J. T. Hynes, J. Chem. Phys. **73** (1980) 2700.
51. S. Nordholm, Chem. Phys. **137** (1989) 109.
52. D. M. Leitner and P. G. Wolynes, Chem. Phys. Lett. **280** (1997) 411.
53. H. Wang, L. Zhu, and W. L. Hase, J. Phys. Chem. **98** (1994) 1608.
54. W. L. Hase, R. J. Duchovic, X. Hu, A. Komornicki, K. F. Lim, D.-H. Lu, G. H. Peslherbe, K. N. Swamy, S. R. Vande Linde, A. Varandas, H. Wang, and R. J. Wolf, Quant. Chem. Prog. Exch. Bull. **16** (1996) 671.
55. X. Hu, W. L. Hase, and T. Pirraglia, J. Comput. Chem. **12** (1991) 1014.
56. W. L. Hase and D. G. Buckowski, Chem. Phys. Lett. **74** (1980) 284.
57. U. Lourderaj, J. L. McAfee, and W. L. Hase, J. Chem. Phys. **129** (2008) 094701, Appendix A.
58. K. Bolton, W. L. Hase, and G. H. Peslherbe, Direct Dynamics Simulations of Reactive Systems, in: *Modern Methods for Multidimensional Dynamics Computations in Chemistry*, D. L. Thompson (Ed.), World Scientific, Singapore (1998), pp. 143.
59. L. Sun and W. L. Hase, Rev. Comput. Chem. **19** (2003) 79.
60. W. L. Hase, K. Song, and M. S. Gordon, Comput. Sci. Eng. **5** (2003) 36.
61. M. Valiev, E. J. Bylaska, N. Govind, K. Kowalski, T. P. Straatsma, H. J. J. van Dam, D. Wang, J. Nieplocha, E. Apra, T. L. Windus, and W. A. de Jong, Comput. Phys. Commun. **181** (2010) 1477.
62. M. Valiev, E. J. Bylaska, N. Govind, K. Kowalski, T. P. Straatsma, H. J. J. Van Dam, D. Wang, J. Nieplocha, E. Apra, T. L. Windus, and W. A. de Jong, Comput. Phys. Commun. **181** (2010) 1477.
63. R. Wester, A. E. Bragg, A. V. Davis, and D. M. Neumark, J. Chem. Phys. **119** (2003) 10032.
64. B. S. Rabinovitch and D. W. Setser, Adv. Photochem. **3** (1964) 1.
65. G. H. Peslherbe, H. Wang, and W. L. Hase, J. Chem. Phys. **102**, (1995) 5626.
66. N. B. Slater, *Theory of Unimolecular Reactions*, Cornell University, Ithaca, (1959), pp. 19.
67. S. R. Vande Linde and W. L. Hase, J. Chem. Phys. **93** (1990) 7962.
68. J. Mikosch, R. Otto, S. Trippel, C. Eichhorn, M. Weidemüller, and R. Wester, J. Phys. Chem. **112** (2008) 10448.
69. C. Li, P. Ross, J. E. Szulejko, and T. B. McMohan, J. Am. Chem. Soc. **118** (1996) 9360.
70. D. S. Tonner and T. B. McMahon, J. Am. Chem. Soc. **122** (2000) 8783.
71. L. Sun, W. L. Hase, and K. Song, J. Am. Chem. Soc. **123** (2001) 5753.
72. Y. J. Cho, S. R. Vande Linde, L. Zhu, and W. L. Hase, J. Chem. Phys. **96** (1992) 8275.